The microstructure and electrical properties of nonalloyed epitaxial Au-Ge ohmic contacts to *n*-GaAs

H. S. Lee, M. W. Cole, R. T. Lareau, S. N. Schauer, D. C. Fox, D. W. Eckart, R. P. Moerkirk, W. H. Chang, and K. A. Jones
Electronics Technology and Devices Laboratory, U.S. Army, Fort Monmouth, New Jersey 07703-5601

S. Elagoz, W. Vavra, and R. Clarke
The Harrison M. Randall Laboratory of Physics, University of Michigan, Ann Arbor, Michigan 48109

(Received 30 April 1992; accepted for publication 6 August 1992)

The microstructure and electrical properties of nonalloyed epitaxial Au-Ge contacts were studied. Ohmic behavior was obtained after a 3 h anneal at 320 °C with the lowest average contact resistance and specific contact resistivity found to be $\sim 0.28\ \Omega$ mm and $\sim 7\times 10^{-6}$ $\Omega\ cm^2$, respectively. Localized reactions in the form of islands were observed across the surface of the contact after annealing and were composed of Au, Ge, and As, as determined by secondary ion mass spectroscopy (SIMS) imaging and Auger depth profiling. Back side SIMS profiles indicate deep Ge and Au diffusion into the GaAs substrate in the island regions. Ohmic contact behavior was found to depend upon both the kinetics of the reactions (localized reactions and island growth) and the thermodynamics (substantial diffusion of both Au and Ge) of the system. A model describing the coupled Au and Ge in-diffusion with respect to the GaAs substrate is presented.

INTRODUCTION

Ohmic contacts to *n*-GaAs for electronic and optoelectronic devices and circuits have traditionally been Au-Ge based systems and much work has been devoted to the understanding of this contact system and the metal-semiconductor reactions contained therein.[1] Typically, these contacts have been formed by evaporation of Au, Ge, (or an Au-Ge alloy) and Ni films with a subsequent anneal above the 356 °C Au-Ge eutectic temperature.[2] It is well known that this alloying process not only alters the physical and chemical structure of the deposited films it also introduces interfacial roughness and potential spiking problems.[3] In addition, these contacts were often formed on GaAs with a thin surface oxide and were microstructurally polycrystalline. These variables have made it extremely difficult to study the fundamental mechanisms of ohmic contact formation in a controlled fashion. We have collectively addressed these problems by using a greatly simplified system: nonalloyed Au-Ge ohmic contacts using a single crystal Ge film grown on an oxide free GaAs surface under ultrahigh vacuum (UHV) conditions. A nonalloyed contact provides smoother interface morphology and can be used with shallow junctions. Nonalloyed ohmic contacts have been made in the past by sintering,[4,5] growing heavily doped GaAs,[6,7] and using As-doped epitaxial Ge films on GaAs.[8,9] The Au and the Ge were both deposited under UHV conditions and should therefore yield reduced interfacial contamination and diminished grain boundary diffusion. The reduction of oxygen may be important since oxygen on the GaAs surface has been observed to decrease the rate of reactions in the Pd/GaAs and Pt/GaAs systems.[10,11] Such a system will allow us to further explore the fundamental mechanisms of ohmic contact formation and to compare the results with studies using polycrystalline films.[12]

The Au/Ge interactions with GaAs and resulting microstructure were investigated using scanning electron microscopy (SEM), Auger electron spectroscopy (AES), transmission electron microscopy (TEM), and front-side and back-side secondary ion mass spectroscopy (SIMS). Electrical performance was evaluated using transmission line model (TLM) measurements on contact pads with varying gaps.

EXPERIMENT

The sample structure consisted of 500 Å Au/250 Å Ge/GaAs substrate. First, the samples were cleaned in warm solvents and then loaded into a Vacuum Generators® V-80 M molecular beam epitaxy (MBE) system with a base pressure $<8\times 10^{-11}$ Torr. Prior to Ge growth the samples were annealed at 590–600 °C for 20–40 min to remove the surface oxide. 250 Å Ge was grown using an electron beam hearth at a rate of $\sim$0.2–0.3 Å/s at 400 °C. The sample was then cooled to 100 °C and Au was then deposited at a rate of $\sim$0.08 Å/s using a Knudsen Cell heated to 1300 °C. The Ge was epitaxial with respect to the GaAs substrate, and the Au was highly oriented as determined by x-ray diffraction, reflection high energy electron diffraction (RHEED), and selected area electron diffraction. A conventional furnace with an Ar ambient was used to anneal the contacts at 320 °C for various times.

A PHI 660 scanning Auger microprobe was utilized for compositional and structural analysis. A 4 keV Ar^+ ion beam was used for sputter depth profiling. The base pressure of the instrument was $\sim 3\times 10^{-10}$ Torr, with the pressure during the analysis rising to $\sim 5\times 10^{-8}$ Torr. The impact energy of the electron beam was 10 keV. The sample was tilted $\sim 30°$ from normal incidence of the electron column. The high resolution TEM was performed on a

 © 1992 American Institute of Physics

JEOL 2010. An AMRAY 1610 SEM was used for surface analysis.

While front-side SIMS and Auger microprobe analyses may provide compositional information in the metallization region above the substrate very little can be understood below the metal/substrate interface due to effects such as ion beam mixing, surface/interface roughness, and preferential sputtering. The SIMS back-side sputter depth profile technique overcomes these difficulties and enables high depth resolution measurements to be made since diffusion profiles are measured from low to high concentration gradients. The SIMS back-side sputter depth profile technique was first used successfully to study alloyed AuGeNi and TiB_2 ohmic contacts[13,14] and has been used to analyze a variety of ohmic and Schottky contacts.[15–17] For the diffusion study using the back-side SIMS technique, marker layers were used to monitor depth in the sample and were first grown in a Varian GEN II MBE system. The following structure was grown by MBE on semi-insulating (SI) (100) GaAs:$Al_{0.3}Ga_{0.7}As$ (1.0 μm)/GaAs (undoped 2000 Å)/GaAs (n-type, Si-doped 1×10^{18} cm^{-3}, 2000 Å)/10×[GaAs (n-type, Si-doped 1×10^{16} cm^{-3}, 500 Å)/GaAs (n-type, Si-doped 1×10^{18} cm^{-3}, 500 Å)]. The $Al_{0.3}Ga_{0.7}As$ layer was used as an etch stop in the removal of the GaAs substrate. The Au and Ge layers were then deposited as described above. Sample preparation details for the back-side SIMS technique are given elsewhere.[18] In order to make electrical contact to the SIMS sample holder the sample was gold-coated after the back-side preparation. A Cameca IMS-3F secondary ion mass spectrometer was used for this study. The primary ion beam was mass-filtered Cs^+ with a net impact energy of 14.5 keV. Negative secondary ions were analyzed to maximize signal intensity. The vacuum in the sample chamber during analysis was $\sim5\times10^{-8}$ Torr.

For electrical analysis transmission line model (TLM) patterns were simultaneously fabricated on Au/Ge layers grown on an n^+ (Si-doped 1×10^{18} cm^{-3}, 1.0 μm) epilayer on SI GaAs. The TLM pattern processing included a two-step chemical etch of the Au and Ge layers using KI/I_2 and H_2O_2, respectively.

RESULTS

Ohmic behavior of the contacts was observed only after annealing at 320 °C for 3 h. For these conditions specific contact resistivity and contact resistance measurements on TLM patterns yielded average values as low as 7×10^{-6} Ω cm^2 and 0.28 Ω mm, respectively. This compares quite favorably with our previous study using polycrystalline films[12] (5×10^{-6} Ω cm^2) and is lower than the nonalloyed polycrystalline Au-Ge contacts achieved by others.[5] The contacts were found to be fairly stable at 320 °C, increasing to $\sim2\times10^{-5}$ Ω cm^2 after 21 h as seen in Fig. 1. The contact resistance remained at the value of 0.28 Ω mm.

Figure 2 shows SEM micrographs of contacts in the as-deposited state, and after 1, 2, and 3 h anneals at 320 °C. The formation of islands on the surface of the contact is apparent after 1 h, and the size and density of these islands

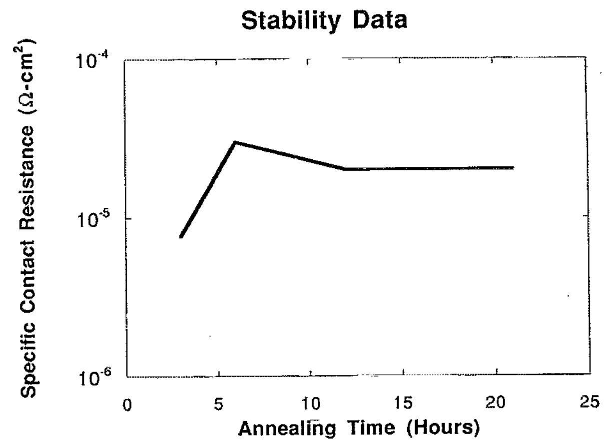

FIG. 1. Specific contact resistance of epitaxial Au-Ge ohmic contact annealed at 320 °C plotted as a function of anneal time.

increase with annealing time. A plot of the ratio of island area to total area as a function of anneal time at 320 °C is presented in Fig. 3. The curve flattens out after about 3 h, which is roughly the time required to achieve an ohmic contact.

The AES depth profile for the as-deposited Au/Ge/GaAs structure showed a broad interface between the Ge layer and the GaAs as seen in Fig. 4. After annealing for 1 h the contact surface appeared spotted with dark, island-like regions about 3–5 μm in length. Auger depth profiles were obtained inside and outside these localized island regions and are shown in Figs. 5(a) and 5(b), respectively. Figure 5(a) shows the Auger depth profile for this contact after the 1 h anneal inside the localized region. Substantial Ge and As interdiffusion were observed, with the appearance of a GeAs type phase near the surface, and the initial formation of two Ge layers beneath that layer. Ga out-diffusion to the surface was also observed with evidence of limited compound formation in the Au layer in Fig. 5(a).

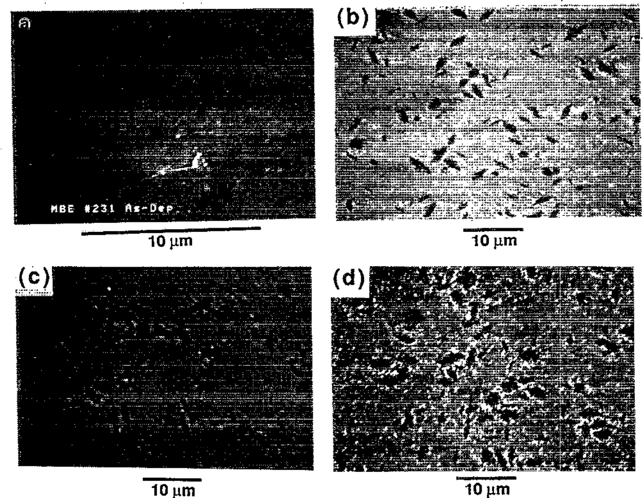

FIG. 2. SEM micrographs of epitaxial Au-Ge contact surface after increasing anneal times at 320 °C: (a) as-deposited, (b) 1 h, (c) 2 h, (d) 3 h.

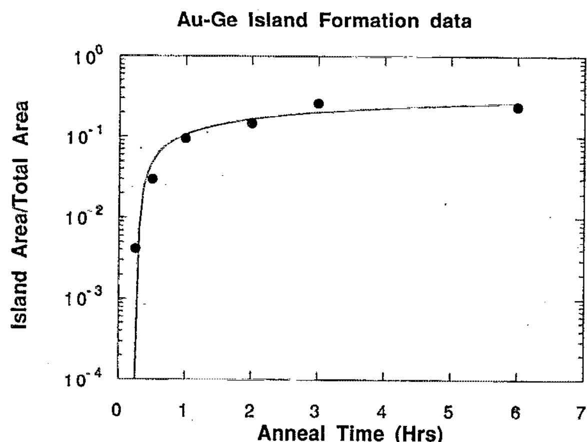

FIG. 3. Ratio of island area to total area of contact plotted as a function of anneal time.

This is seen in the small rise in the Ga signal near 5 min with a reacted thickness on the order of ~50 Å. Au diffusion appears limited to the GaAs substrate region. The AES depth profile outside the localized island regions for this contact is shown in Fig. 5(b). This profile indicated very little interaction between the Au-Ge and the GaAs and essentially resembled the as-deposited case of Fig. 4. Increased Au, Ge, As, and Ga diffusion was observed after a 2 h anneal as seen in the AES depth profile inside an island presented in Fig. 6. Again, very little interaction was observed outside the islands and therefore the depth profile is not presented.

Figure 7 shows the AES depth profile inside an island of the contact after a 3 h anneal, which resulted in an ohmic contact. Auger analysis of this region showed the complete formation of the Ge layer on the GaAs substrate. The GeAs type layer near the surface appears to be stable, and the contact possesses two distinct Ge layers, separated by a second thin GeAs type layer. The onset of ohmic behavior coincides with the complete formation of the Ge layer on the GaAs. Ga out-diffusion is still evident al-

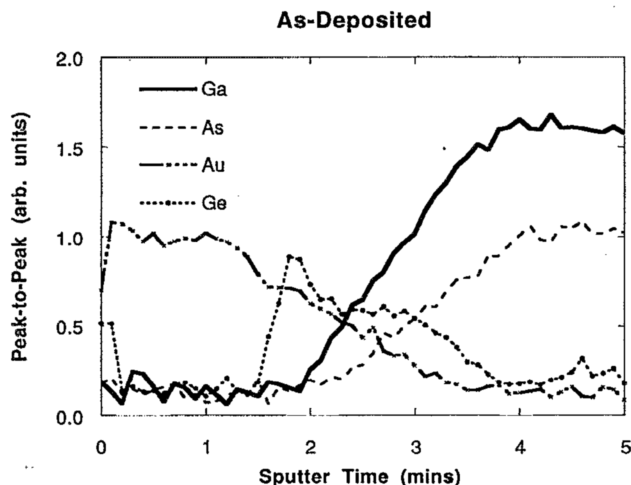

FIG. 4. AES depth profile for as-deposited Au-Ge sample.

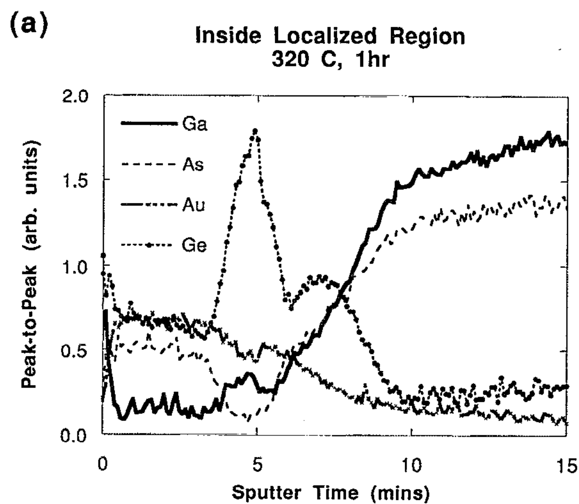

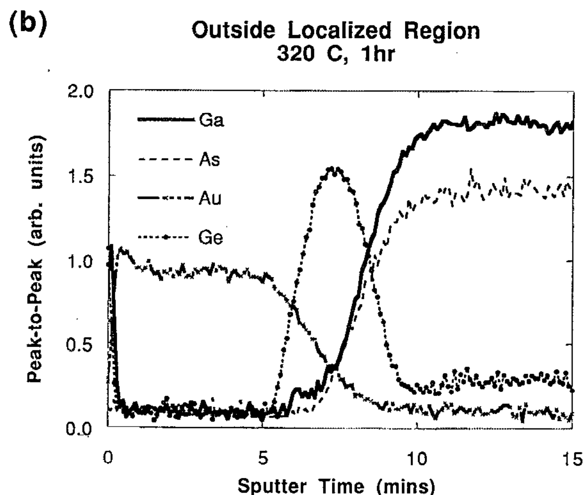

FIG. 5. AES depth profiles for Au-Ge contact after 320 °C anneal for 1 h: (a) inside island region, (b) outside island region.

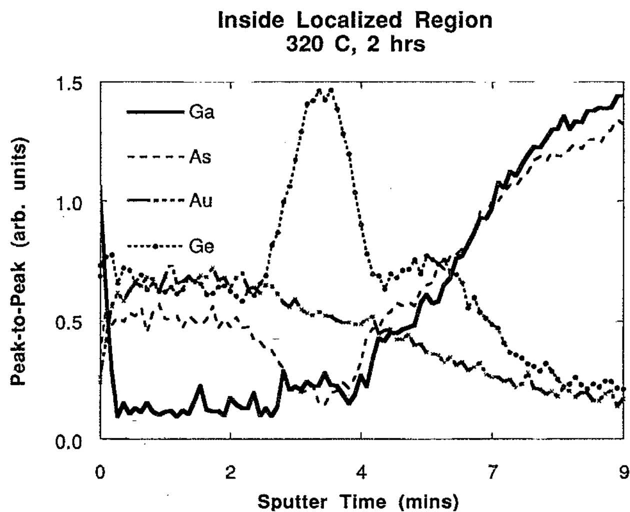

FIG. 6. AES depth profile for Au-Ge contact inside island region after 320 °C anneal for 2 h.

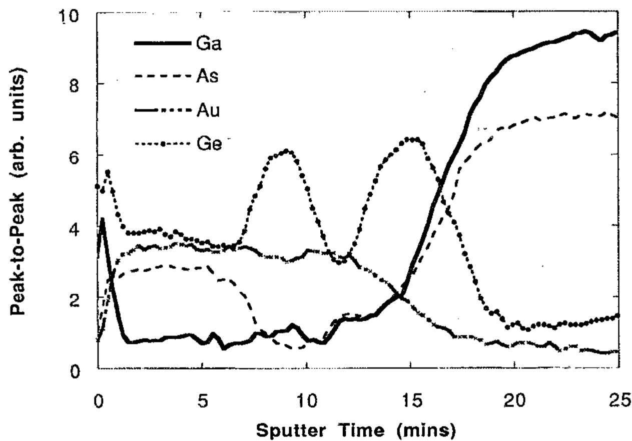

FIG. 7. AES depth profile for Au-Ge contact inside island region after 320 °C anneal for 3 h.

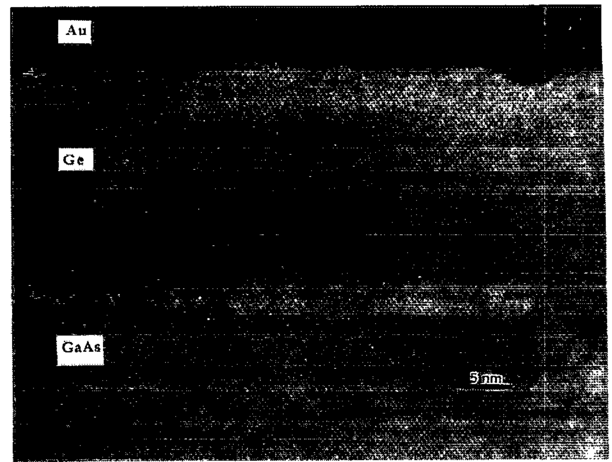

FIG. 9. High resolution TEM micrograph outside the island regions of epitaxial Au-Ge contact. The interfaces are denoted by arrows. The contact was annealed at 320 °C for 3 h.

though the extent of Ga interaction with the Au layer near 12 min cannot be accurately determined. In comparison, there was little As detected and no evidence of GeAs phase formation in the localized regions of the previously studied polycrystalline contact structure.[12] As in the case after the 2 h anneal, the Auger depth profile after the 3 h anneal was similar to that of the as-deposited sample.

Cross-sectional TEM revealed roughness at the Ge/GaAs interface on the order of 300 Å and regions where the Au was in contact with the GaAs. This is shown in Fig. 8. This broadness in the interface was substantiated by the Auger analysis in Fig. 4. The average depth of the Au protrusions was ~70 Å with the deepest protrusion of ~450 Å. Due to growth nonuniformities, this may not be representative of the entire wafer. The Au film is composed of highly textured, large grains. The orientation relationship as determined by selective area diffraction was found to be Au⟨200⟩‖ Ge ⟨220⟩‖ GaAs ⟨220⟩. Figure 9 shows a high resolution TEM micrograph of an area outside the islands after a 3 h anneal. The analysis revealed very limited reaction between the Au-Ge and GaAs. Structurally, a clean Ge/GaAs interface can be seen, as well as a fairly smooth Au/Ge interface. The Au layer is highly oriented with respect to the Ge and the GaAs with the same orientational relationship as the as-deposited sample: Au⟨200⟩‖ Ge ⟨220⟩‖ GaAs ⟨220⟩. These TEM results are consistent with the Auger analysis outside the localized region after the 3 h anneal. The results differ from the previously studied polycrystalline Au-Ge contacts where the Au orientation on the GaAs was determined to be Au⟨111⟩‖ GaAs ⟨100⟩. This difference is due in part to the absence of the native oxide for the epitaxial contacts.

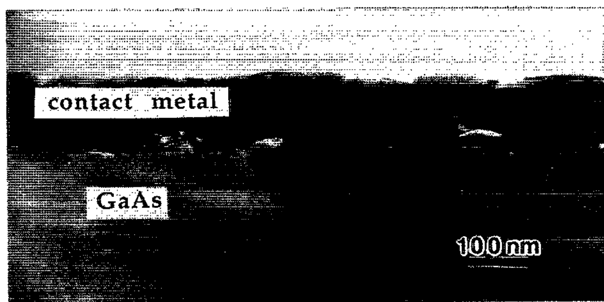

FIG. 8. TEM micrograph of as-deposited Au-Ge sample.

Figure 10(a) shows a front-side SIMS depth profile of the as-deposited Au/Ge/GaAs sample on the substrate containing the Si-doped marker layers. The Au and Ge signals can be seen with their respective tails into the GaAs substrate. Note that these tails are artifacts caused by ion beam mixing and sputtering effects. The second Au peak at the Ge/GaAs interface is due to ionization effects and the oscillations in the Si signal are due to the Si concentration changes in the marker layers. A front-side depth profile of a sample which exhibited ohmic behavior after being annealed at 320 °C for 3 h is shown in Fig. 10(b). Comparison with Fig. 10(a) indicates clearly that there has been diffusion of As and Ge into the Au layer as seen in the relative rise in the Ge and As signals near 200 s. Ga signals are not shown due to the relatively low Ga sensitivity using Cs^+ as a primary beam. Since the sputter rate differed in the two depth profiles, the axes are scaled to similar depths using the Si marker layers.

A back-side SIMS depth profile of the as-deposited sample is shown in Fig. 11(a). Note that the surface is now on the right-hand side of the graph. A more accurate measurement of the Au and Ge distribution is illustrated by the sharp rise in the Au and Ge signals in Fig. 11(a) in contrast to the Au and Ge tails caused by ion beam mixing in Fig. 10(a). Note also in Fig. 11(a) the absence of the second Au peak which was observed in Fig. 10(a) due to an ionization artifact. The marker layers of 1000 Å periodicity can be seen in the Si signal intensity oscillations. Figure 11(b) depicts the back-side imaging profile of the sample annealed at 320 °C for 3 h. The stable As matrix

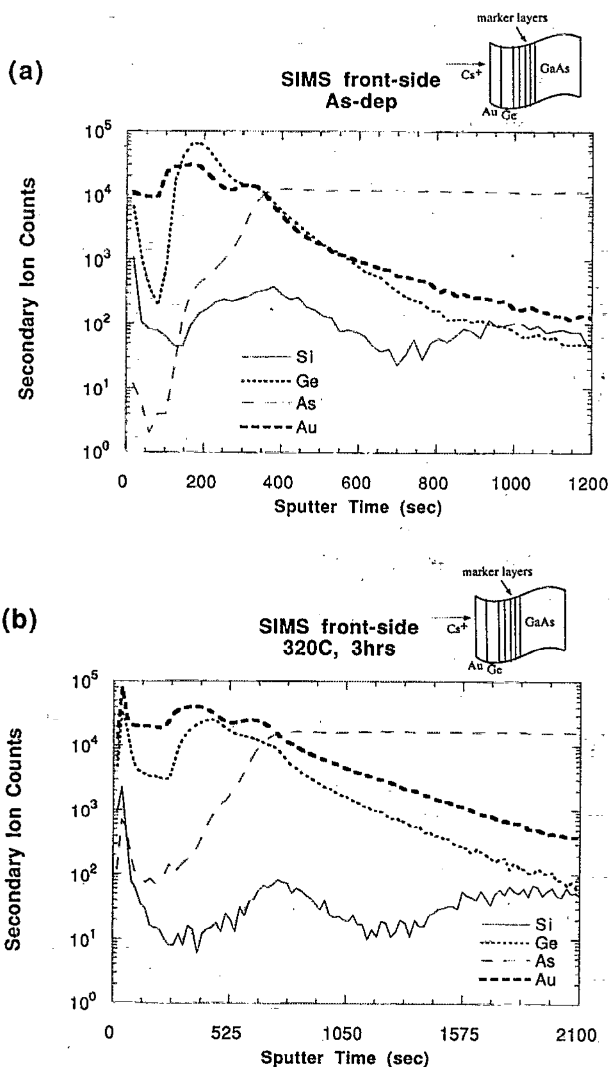

FIG. 10. SIMS front-side depth profiles: (a) as-deposited sample, (b) after 320 °C anneal for 3 h.

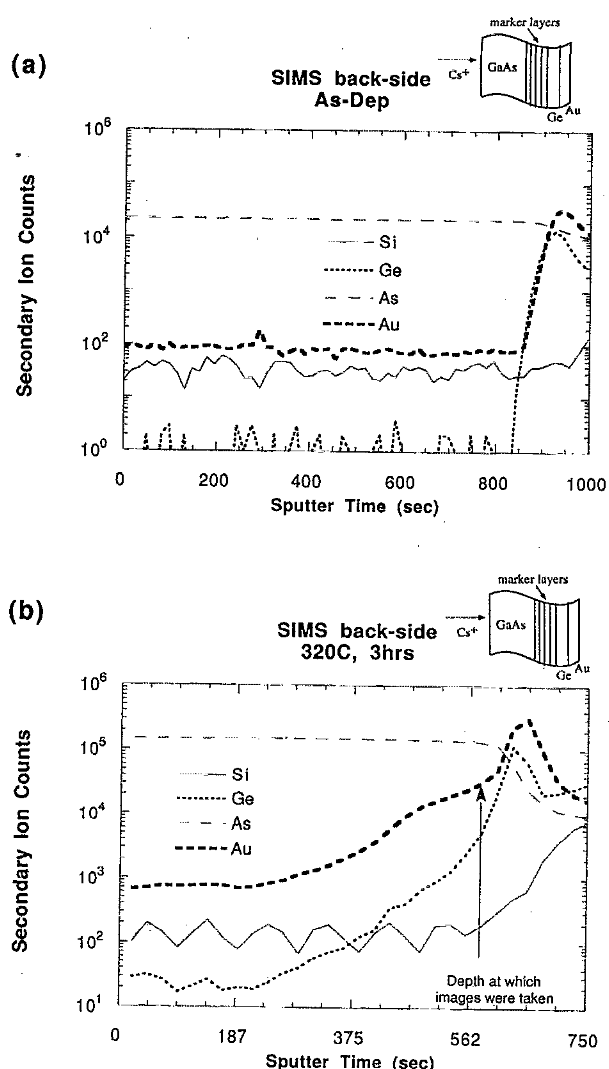

FIG. 11. SIMS back-side depth profiles: (a) as-deposited sample, (b) after 320 °C anneal for 3 h.

signal from the substrate up to the contact interface implies little substrate change as a result of the anneal. The Si marker layers indicate that any substrate consumption is probably less than 500 Å. The high sensitivity of this back-side technique allows for the determination of trace levels of Au and Ge. As in the front-side profiles, Au and Ge diffusion are apparent when Figs. 11(a) and 11(b) are compared. Au is observed to penetrate approximately 4500 Å into the GaAs substrate. The Ge signal possesses a much sharper rise near 600 s with a diffusion distance that is nearly the same (4000 Å) as that of Au. The back-side lateral images corresponding to Fig. 11(b) are shown in Fig. 12. At this depth just below the substrate region Au and Ge both exhibit similar segregation effects, indicating coupled localized reactions for both Au and Ge.

It should be stressed that Fig. 11(b) represents an average of the signals inside and outside the island regions. Selected area profiles corresponding to Fig. 11(b) for Au are shown in Figs. 13(a) and 13(b). The profiles show substantial differences between Au diffusion inside and outside the island regions. A plateau in the Au signal near 500 s is apparent inside the island region which could possibly indicate a Au-Ga reaction. The penetration depth for this plateau appears to be ~2000 Å. Au penetration is substantially less outside the island region. Figure 13(b) shows the selected area profiles for Ge. The Ge signal does not exhibit the same plateau as Au in Fig. 13(a) in the localized region. Again, there is a distinctly greater Ge diffusion (~1000 Å) inside the island region than outside of it.

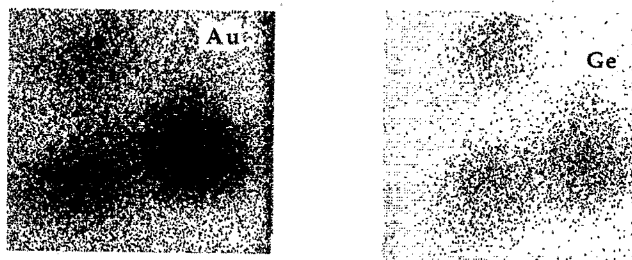

FIG. 12. Back-side lateral images for sample annealed at 320 °C for 3 h.

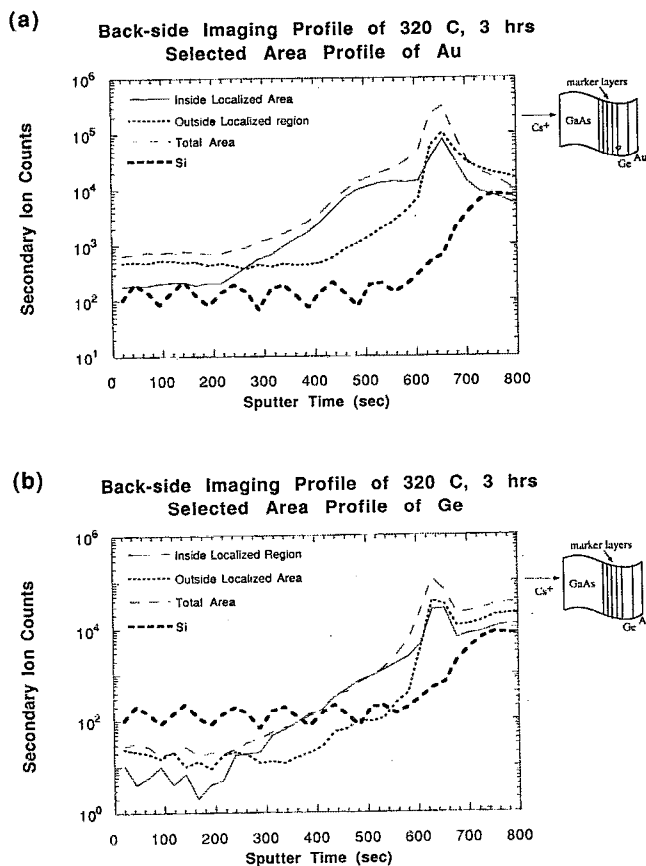

FIG. 13. Selected area profiles using back-side SIMS for (a) Au and (b) Ge in the contact after annealing at 320 °C for 3 h. (a) and (b) show profiles inside and outside the island regions, profiles over the total area, and profiles of the Si marker layers.

DISCUSSION

The formation of an epitaxial nonalloyed ohmic contact may be looked upon from roughly two points of view: kinetics or thermodynamics. The kinetics perspective would explain the island formation and segregation effects while the thermodynamics analysis could describe the phase formations within these islands. Au-Ge island formation data of Fig. 3 correlated with contact resistivity results (Fig. 1) provide some evidence that ohmic contact behavior must be accompanied by some critical island or localized region density. This saturation of the island formation/density factor suggests the possibility of a lateral diffusion-limited process. Further, since the contact structure is epitaxial, the resistivity will not be dominated by grain boundary diffusion as in the case of polycrystalline contacts.[19] Our results suggest that localized reactions or island formation are important in achieving a nonalloyed Au-Ge ohmic contact. Localized reactions in the nonalloyed Au-Ge ohmic contact system have been observed in a previous study.[12] There, it was also determined that a contact composed exclusively of Ge/GaAs was not ohmic. Iladis and Singer[20] pointed out the significance of the inhomogeneous lateral Ge distribution in the ultimate formation of an alloyed ohmic contact while Braslau[3,21] proposed a contact model for the alloyed Au/Ni/Ge system where conduction occurs in the Ge-rich islands. In our study the SEM and lateral SIMS images (Figs. 2 and 12), the SIMS, and AES depth profiles combine to clearly show the segregation of Ge and As to the same localized regions above the substrate and the segregation of Ge and Au to the same localized regions at the contact/GaAs substrate interface. TEM results for the as-deposited structure in Fig. 8 reveal Au protrusions into the GaAs substrate which may serve as nucleation sites for the localized reactions. Previous work[22,23] on Au-GaAs reactions have also documented the lateral inhomogeneity of Au on GaAs but the temperatures used were above the Au-Ga eutectic of 347 °C.[24] The simplified epitaxial Au/Ge/GaAs contact structure results in a system that is dependent upon segregation and island formation for ohmic behavior.

A thermodynamic analysis of the epitaxial contact may describe the actual compound phase formation that takes place within the islands or localized regions. While microstructural results for contacts annealed for 3 h at 320 °C showed that the Ge/GaAs interface is smooth outside the island regions as in Fig. 9, inside the island region there is substantial Au and Ge interdiffusion. The Auger profiles in Fig. 5(a) illustrate this substantial Ge, As, Au, and Ga diffusion in the localized regions after only 1 h of annealing. There is substantial Au in-diffusion only in the localized regions as seen in the back-side lateral images in Fig. 12. This Au in-diffusion is accompanied by rapid in-diffusion of Ge. The resultant Ge diffusion behavior at the Ge/GaAs interface can be seen in the evolution of different Ge/As-related phases from the Auger and back-side SIMS profiles. The incorporation of both Au and Ge in the substrate region has been seen in this study to be necessary for ohmic behavior and we consider the Au and Ge related phase formation below.

The Au interaction with Ga in Figs. 5(a), 6, and 7 appears to be limited to reaction thicknesses less than 50 Å. However, the penetration of Au into the GaAs substrate over time is more carefully observed in the back-side SIMS profile in Fig. 13(a). The Au in this localized region of a contact which displayed ohmic behavior (320 °C, 3 h) exhibits a plateau just beneath the metal/GaAs interface, indicative of a possible reaction with the GaAs. Au is a known interstitial diffuser in GaAs[25,26] and has been shown to enhance Ge in-diffusion due to excess Ga vacancies in sintered Au-Ge contacts.[4] In addition it is known from thermochemical data[27] that AuGa ($\Delta H \sim -7.64$ kcal/mol) compound formation is favored over AuGe ($\Delta H \sim -2.24$ kcal/mol). The dissolution of Au in GaAs then may best be studied to first order using a ternary phase diagram. The Au-Ga-As ternary phase diagram shown in Fig. 14(a) as derived by Byers *et al.*[28] reveals that the phases AuGa-GaAs-Au can exist and are stable thermodynamically. The existence of such a AuGa-GaAs-Au system could also explain the limited Au interaction with Ga above the contact.

Ge interdiffusion is influenced to a great extent by Au in-diffusion. The formation of stable AuGa phases just beneath the metal/GaAs interface may promote the incorporation of Ge since Ge is known to diffuse substitutionally.[29]

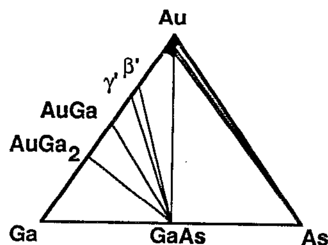

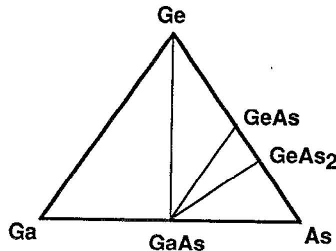

FIG. 14. Ternary phase diagrams: (a) Ga-As-Au and (b) Ga-As-Ge. Both are valid for $300 < T < 600$ °C and are taken from Ref. 28.

The selected area profile [Fig. 13(b)] shows the greater Ge diffusion into the GaAs in the island regions. However, while this incorporation of Ge may suggest heavy doping of the GaAs substrate region it does not eliminate the possibility of a thin graded Ge/GaAs layer or a Ge/GaAs heterojunction as was considered for Ge/Pd contacts.[15] This is supported in part by examination of the Ge-Ga-As ternary phase diagram in Fig. 14(b). Tie-lines can be drawn between the stable phases Ge-GaAs-GeAs (or $GeAs_2$). The Ge/GaAs region could accommodate these phases which would allow for the existence of the required heterojunction. The Ge-Ga-As phase diagram indicates the existence of the different Ge-related phases that are present in the localized island regions with the onset of ohmic behavior in the Auger profiles. The evolution of the Ge layer into the GeAs phases and the Ge phases may be now seen in the following manner. Rapid Ge and As out-diffusion to the contact surface away from the substrate initially occurs, resulting in GeAs formation. The rapid Ge diffusion may be due to the Au in-diffusion while As is a known diffuser in Ge[9] and Au.[30] As the As out-diffusion diminishes Ge diffusion into the GaAs dominates. The reason for this behavior may be due in part to the formation of the thin (50 Å) AuGa diffusion barrier as was observed in Fig. 5(a) near 5 min. This would serve to limit As out-diffusion and, in the absence of such diffusion, would allow Ge in-diffusion to occur.

A model that emerges for this single crystal ohmic contact formation is as follows. Au first comes in contact with the GaAs at points where the Ge layer is either very thin or nonexistent. It reacts with the GaAs to form AuGa phases which results in the formation of free As and/or vacancies in the GaAs lattice. The Ge then rapidly indiffuses substitutionally via Ga vacancies forming GeAs related phases. Heavy Ge doping may then occur, leading to ohmic contact formation.

CONCLUSION AND SUMMARY

Nonalloyed Au-Ge ohmic contacts were formed using single crystal Ge grown on GaAs. SEM, AES depth profiles, and SIMS imaging revealed localized reactions across the contact surface, with substantial Ge, Ga, and As interdiffusion in the localized island regions. Two factors are important in ohmic contact formation: localized reactions and island growth, and the substantial diffusion of both Au and Ge. The ohmic contact can be modeled as a coupled Au and Ge interaction with the GaAs. The lowest average contact resistance and specific contact resistivity were found to be $\sim 0.28\ \Omega$ mm and $\sim 7 \times 10^{-6}\ \Omega\, cm^2$, respectively.

ACKNOWLEDGMENTS

The authors gratefully acknowledge A. DeAnni, P. Newman, and R. Khana for their assistance.

[1] See for example, C. J. Palmstrøm and D. V. Morgan, in *Gallium Arsenide: Materials, Devices, and Circuits*, edited by M. J. Howes and D. V. Morgan (Wiley, New York, 1985), p. 195.
[2] M. Hansen, *Constitution of Binary Alloys* (McGraw-Hill, New York, 1958), p. 207.
[3] N. Braslau, J. Vac. Sci. Technol. A **4**, 3085 (1986).
[4] O. Aina, W. Katz, B. J. Baliga, and K. Rose, J. Appl. Phys. **53**, 777 (1982).
[5] J. G. Werthen and D. R. Scifres, J. Appl. Phys. **52**, 1127 (1981).
[6] P. D. Kirchner, T. N. Jackson, G. D. Pettit, and J. M. Woodall, Appl. Phys. Lett. **47**, 26 (1985).
[7] P. A. Barnes and A. Y. Cho, Appl. Phys. Lett. **33**, 651 (1978).
[8] W. J. Devlin, C. E. C. Wood, R. Stall, and L. F. Eastman, Solid-State Electron. **23**, 823 (1980).
[9] R. A. Stall, C. E. C. Wood, K. Board, N. Dandekar, L. F. Eastman, and J. Devlin, J. Appl. Phys. **52**, 4062 (1981).
[10] D. H. Ko and R. Sinclair, Appl. Phys. Lett. **58**, 1851 (1991).
[11] T. S. Kuan, J. L. Freeouf, P. E. Batson, and E. L. Wilkie, J. Appl. Phys. **48**, 402 (1986).
[12] M. A. Dornath-Mohr, M. W. Cole, H. S. Lee, D. C. Fox, D. W. Eckart, L. Yerke, C. S. Wrenn, R. T. Lareau, W. H. Chang, K. A. Jones, and F. Cosandey, J. Electron. Mater. **19**, 1247 (1990).
[13] J. R. Shappirio, R. T. Lareau, R. A. Lux, J. J. Finnegan, D. D. Smith, L. S. Heath, and M. Taysing-Lara, J. Vac. Sci. Technol. A **5**, 1503 (1987).
[14] R. T. Lareau, in *SIMS VI*, edited by A. Benninghoven, A. M. Huber, and H. W. Werner (Wiley, New York, 1988), p. 437.
[15] C. J. Palmstrøm, S. A. Schwarz, E. D. Marshall, E. Yablonovitch, J. P. Harbison, C. L. Schwarz, L. Florez, T. J. Gmitter, L. C. Wang, and S. S. Lau, in *Advanced Surface Processes for Optoelectronics*, Proc. 67, edited by S. Bernasek, T. Venkatesan, and H. Temkin (Material Research Society, Pittsburgh, PA, 1988) p. 283.
[16] C. J. Palmstrøm, S. A. Schwarz, E. Yablonovitch, C. L. Schwarz, L. Florez, T. J. Gmitter, E. D. Marshall, and S. S. Lau, J. Appl. Phys. **67**, 334 (1990).
[17] S. A, Schwarz, C. J. Palmstrøm, C. L. Schwarz, T. Sands, L. G. Shantharama, J. P. Harbison, L. Florez, E. D. Marshall, C. C. Han, and S. S. Lau, J. Vac. Sci. Technol. A **8**, 2079 (1990).
[18] H. S. Lee, R. T. Lareau, S. N. Schauer, R. P. Moerkirk, K. A. Jones, S. Elagoz, W. Vavra, and R. Clarke, in *Advanced III-V Compound Semiconductor Growth, Processing and Devices*, Proc. 240, edited by S. J. Pearton, J. M. Zavada, and D. K. Sadana (Materials Research Society, Pittsburgh, PA, 1992), p. 473.
[19] C. R. M. Grovenor, *Microelectronic Materials* (Adam Hilger, Bristol, 1989), p. 196.

[20] A. Iladis and K. E. Singer, Solid State Commun. **49**, 99 (1984).
[21] N. Braslau, J. Vac. Sci. Technol. **19**, 803 (1981).
[22] L. L. Yeh and P. H. Holloway, in *Advances in Materials, Processing and Devices in III-V Compound Semiconductors*, Proc. 144, edited by D. K. Dadana, L. F. Eastman, and R. Dupuis (Materials Research Society, Pittsburgh, PA, 1988), p. 607.
[23] V. G. Weizer and N. S. Fatemi, J. Appl. Phys. **64**, 4618 (1988).
[24] C. J. Cooke and W. Hume-Rothery, J. Less Common Metals **10**, 42 (1966).
[25] D. Shaw, *Atomic Diffusion in Semiconductors* (Plenum, New York, 1973).
[26] V. I. Sokolov and F. S. Shishiyanu, Sov. Phys. Solid State **6**, 265 (1964).
[27] O. Kubaschewski and C. B. Alcock, *Metallurgical Thermochemistry* (Pergamon, Oxford, 1979).
[28] R. Byers, K. B. Bum, and R. Sinclair, J. Appl. Phys. **61**, 2195 (1987).
[29] M. Ogawa, J. Appl. Phys. **51**, 406 (1980).
[30] I. Mojzes, T. Sebestyen, and D. Szegethy, Solid-State Electron. **25**, 499 (1982).